Accepted Manuscript

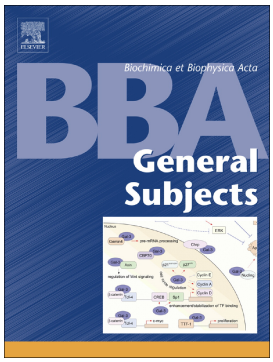

Kinetic evidence for interaction of TMPyP4 with two different G-quadruplex conformations of human telomeric DNA

Cristina Pérez-Arnaiz, Natalia Busto, Javier Santolaya, José M. Leal, Giampaolo Barone, Begoña García

PII: S0304-4165(17)30349-5
DOI: doi:10.1016/j.bbagen.2017.10.020
Reference: BBAGEN 28974

To appear in:

Received date: 16 May 2017
Revised date: 13 October 2017
Accepted date: 27 October 2017

Please cite this article as: Cristina Pérez-Arnaiz, Natalia Busto, Javier Santolaya, José M. Leal, Giampaolo Barone, Begoña García , Kinetic evidence for interaction of TMPyP4 with two different G-quadruplex conformations of human telomeric DNA. The address for the corresponding author was captured as affiliation for all authors. Please check if appropriate. Bbagen(2017), doi:10.1016/j.bbagen.2017.10.020

Kinetic evidence for interaction of TMPyP4 with two different G-quadruplex conformations of human telomeric DNA

Cristina Pérez-Arnaiz,[a] Natalia Busto,[a] Javier Santolaya,[a,b] José M. Leal,[a] Giampaolo Barone[b*] and Begoña García[a*]

[a]Department of Chemistry, University of Burgos, 09001 Burgos, Spain. Email: begar@ubu.es.
[b]Dipartimento di Scienze e Tecnologie Biologiche, Chimiche e Farmaceutiche (STEBICEF), Università degli Studi di Palermo, Viale delle Scienze Ed. 17, 90128, Palermo, Italy. Email: giampaolo.barone@unipa.it

Background
Stabilization of G-quadruplex helices by small ligands has attracted growing attention because they inhibit the activity of the enzyme telomerase, which is overexpressed in more than 80% cancer cells. TMPyP4, one of the most studied G-quadruplex ligands, is used as a model to show that the ligands can exhibit different binding features with different conformations of a human telomeric specific sequence.

Methods
UV-Vis, FRET melting Assay, Isothermal Titration Calorimetry, Time-resolved Fluorescence lifetime, T-Jump and Molecular Dynamics.

Results
TMPyP4 yields two different complexes with two Tel22 telomeric conformations in the presence of Na^+ or K^+. T jump kinetic experiments show that the rates of formation and dissociation of these complexes in the ms time scale differ by one order of magnitude. MD simulations reveal that, in K^+ buffer, "hybrid 1" conformation yields kinetic constants on interaction with TMPyP4 one order lower than "hybrid 2". The binding involves π-π stacking with external loop bases.

Conclusions
For the first time we show that for a particular buffer TMPyP4 interacts in a kinetically different way with the two Tel22 conformations even if the complexes formed are thermodynamically indistinguishable.

General Significance
G-quadruplexes, endowed with technological applications and potential impact on regulation mechanisms, define a new research field. The possibility of building different conformations from same sequence is a complex issue that confers G-quadruplexes very interesting features. The obtaining of reliable kinetic data constitutes an efficient tool to determine reaction mechanisms between conformations and small molecules.

Keywords

Tel22 conformations; TMPyP4; Fast Reactions; Molecular Dynamics

1. Introduction.

The study and advancement of small molecules capable of binding and stabilizing higher-order DNA structures, such as G-quadruplexes, has attracted growing interest.[1] G-quadruplexes can be formed in guanine-rich DNA stretches in the presence of stabilizing ions such as Na^+ or K^+. Although the *in vivo* existence of such structures is still a matter of debate[2], under physiological conditions the human genome contains a large number of potential quadruplex-forming sequences [3,4]. Human telomeric DNA consisting of TTAGGG repeats is an interesting instance of such sequences. Stabilization of telomeric G-quadruplex helices by small ligands is known to inhibit the activity of the enzyme telomerase, which is overexpressed in more than 80% of cancer cells and acts as tumour promoter [5].

In intracellular media, potassium ions abound more than sodium ions, giving way to extensive research of G-quadruplex conformations stabilized by K^+ [6]. The main conformation reported for the human telomeric sequence in K^+ solutions "Tel22" (d[AGGG(TTAGGG)$_3$]) consists of a G-quadruplex fold with (3+1) G-tetrad core containing three tetrads, one side-chain reversal loop and two lateral loops [7]. Two distinguishable conformations (known as Hybrid-1 and Hybrid-2) have been identified containing this core with the same number and type of loops but different loop arrangement [8]. On the other hand, in Na^+ solutions the antiparallel basket-type structure was found for human telomeric DNA. Although this basket form is the only folded conformation fully characterized under these conditions [9], subsequent studies provide evidence for the polymorphism of telomeric sequences in Na^+ solutions, with possible interconversion between various structural forms [10].

In line with these observations, we have reported recently the fast processes that govern different Tel22 structures in equilibrium at 25 ºC. Kinetic T-jump measurements provide evidence for the presence of two G-quadruplex conformations, F1M and F2M, in equilibrium with G-triplex structures, F1'M and F2'M, with M = Na^+ or K^+ [11]. These results, along with other studies, evince the complexity of this system [12–15], thus posing the question of whether small molecules can differentiate between different specific sequence conformations coexisting in solution, a striking feature not reported hitherto. To this aim, we have studied the interaction of Tel22 with the cationic *meso*-tetrakis(N-methyl-4-pyridyl)porphyrin (TMPyP4), capable of stabilizing quadruplex structures and inhibiting the telomerase activity [16]. In spite of being nonselective for

quadruplex helices over duplex DNA [17], TMPyP4 is one of the most studied G-quadruplex ligands ever and its structure has inspired the development of other porphyrin derivatives [18,19]. Nevertheless, certain controversy over the nature of the G-quadruplex/TMPyP4 interactions still remains, and intercalation between adjacent G-tetrads or end-stacking onto the external faces of the G-quadruplex have been proposed [20–22].

Due to its demonstrated affinity with G-quadruplex structures, TMPyP4 has been used in this work as a model molecule to show that certain ligands can exhibit different binding features towards different conformations of a specific sequence. Even though these features can be thermodynamically indistinguishable, they take place at different rates, as suggested recently by J. Lah et al [23] and shown here by T-jump measurements and MD calculations. The F1M/TMPyP4 and F2M/TMPyP4 complexes get formed at low TMPyP4/Tel22 concentration ratio and have very close binding constants ($K_1 = k_f/k_d$), whereas the formation, k_f, and dissociation, k_d, kinetic constants differ considerably. At higher TMPyP4/Tel22 concentration ratio, another type of complex with binding constant K_2 gets formed. This complex has been reported before and is assumed to involve an external mode of binding [24]. This work is a starting point; actually, the interactions of other types of ligands biologically more relevant than TMPyP4 with different oligonucleotides are to be explored in future studies.

2. Materials and methods.

2.1. Sample preparation. The DNA oligonucleotide d[AGGG(TTAGGG)$_3$], known as "Tel22", was purchased from Thermo Fisher Scientific Inc. as dried samples. Stock solutions were prepared with nuclease free water in buffers containing 10 mM Tris-HCl, 1 mM EDTA and 0.15 M of either NaCl or KCl at pH = 7.5 unless otherwise specified. The formation of the G-quadruplex was carried out by incubating for 6 min the oligonucleotide solution at 90 ºC and slowly cooling down (~5 h) to room temperature in order to obtain the thermodynamically equilibrated G-quadruplex structures [13]. Solutions were then stored at 4 ºC overnight to avoid degradation processes and afterwards allow to reach room temperature prior to carry out the measurements. The concentration of the single stranded oligonucleotide was determined by measuring at 90 ºC the absorbance at 260 nm using the absorptivity value of 228500 $M^{-1}cm^{-1}$ provided by the supplier. The double-labelled oligonucleotide FAM-Tel22-TAMRA

(F-Tel22-T) was purchased from Thermo Fisher Scientific Inc. TMPyP4 was supplied by Sigma Aldrich. Stock aliquots of TMPyP4 were prepared in water and stored in the dark at - 20 ºC.

2.2. UV spectroscopy. Spectrophotometric measurements were performed with a HP 8453A photodiode array spectrophotometer (Agilent Technologies, Palo Alto, CA) endowed with a temperature control Peltier system. Titrations were carried out by adding increasing amounts of Tel22 solutions to the TMPyP4 solution in 1 cm path-length cells with black quartz sides at 25ºC. The data were corrected by the dilution factor C^0_D/C_D.

2.3. ITC titrations. Isothermal titration calorimetry (ITC) experiments were performed at 25 ºC using a Nano ITC (TA Instruments, Newcastle, USA). The stirring speed was maintained constant at 250 rpm. The TMPyP4 solution was injected into the calorimetric cell containing the Tel22 solution. Prior to use, all solutions were degassed to reduce to a minimum the formation of bubbles during the experiments. Control experiments were carried out to determine the contribution of the heat of dilution of TMPyP4 and rule out the presence of aggregation processes of the drug that would interfere with the analysis of the ITC data to obtain the TMPyP4/Tel22 thermodynamic parameters. The thermograms (integrated area of the peak/mole of injectant *versus* C_D/C_P ratio) obtained in the titrations were fitted by a "two-site model", as simpler models including the "one-site model" were insufficient to fit the data suitably.

2.4. FRET melting assay. F-Tel22-T was dissolved in water as 100 μM stock solutions and then annealed for 5 min at 0.4 μM concentration at T = 90 ºC in a buffer containing 10 mM KCl or NaCl, 90 mM LiCl and 10 mM lithium cacodylate (LiCaC) at pH = 7.5. Each well of a 96-well plate contained 0.2 μM of F-Tel22-T and different concentrations of TMPyP4. Measurements were performed in a 7500 Real-Time PCR (Applied Biosystems). Readings were performed with excitation at 450-495 nm and detection at 515-545 nm from 25 to 95 ºC at a scan rate of 0.5 ºC/min.

2.5. Time-resolved fluorescence lifetime. Fluorescence lifetime measurements of TMPyP4 were performed both in the absence and in the presence of different amounts of Tel22 in Na+ or K^+ buffer using FLS980 equipment (Edinburg Instruments). The excitation was accomplished at 405 nm using an EPL 405 pulsed diode laser and the emission was collected at 705 nm. Data were analyzed by FAST 3.4.0 software.

2.6. T-Jump measurements. The fast kinetic measurements were performed with a Dialog T-jump instrument built up according to the Riegler et al. prototype [25] in 1.0 cm path-length cells, working in the absorbance mode. The kinetic curves, collected with an Agilent 54622A oscilloscope (Santa Clara, CA, USA), were transferred to a PC and evaluated with the Table Curve program of the Jandel Scientific package (AISN software, Richmond, CA, USA). The time constants were averaged out from 6-fold repeated kinetic experiments.

2.7. Molecular Dynamics. The structures of the Tel22 G-quadruplex in K^+ solution were taken from the *Protein Data Bank*, with PDB id "*2HY9"* for hybrid-1, F1K, and PDB id "*2JPZ"* for hybrid-2, F2K [26]. In detail, the first and last two nucleotides of the G-quadruplex chains of the two PDB id files, both 26-mer hybrids, have been removed to generate the same Tel22 sequence of the experimental studies. The starting molecular structure of TMPyP4 was obtained by full geometry optimization, firstly through semiempirical PM6 calculations [27] and, subsequently, through DFT calculations, using the M06-2X functional [28] in the presence of water as implicit solvent, mimicked by the "conductor-like polarized continuum model" implicit method [29,30]. Atomic partial charges of TMPyP4 were obtained by DFT calculations and force field parameters of TMPyP4 and DNA models were generated with the ACPYPE software (AnteChamber Python Parser interfacE).[31,32] The Amber99SB force field ParmBSC0 nucleic acid torsion parameters were used for the DNA models [33]. A triclinic box of TIP3P water was generated around the G-quadruplex/TMPyP4 system, to a 0.8 nm depth on each side of the solutes, for a total of about 5500 solvent molecules; 39 K^+ ions and 17 Cl^- ions were added to neutralize the DNA negative charge of the sugar- phosphate backbone and to set the solution ionic strength to about 0.15 M.

Explicit solvent molecular dynamics (MD) simulations for F1K/TMPyP4 and F2K/TMPyP4 systems were performed using the Gromacs 5.0.4 software package, [34,35] in the canonical NPT ensemble (for which number of particles, N, pressure, P, and temperature, T, are constant), at 300 K, under control of a velocity-rescaling thermostat [36]. The mesh particle Ewald method was used to describe long-range interactions [37]. Preliminary energy minimizations were run for 5000 steps with the steepest descent algorithm, during which the equilibration of the TMPyP4/G-quadruplex systems were harmonically restrained with a force constant of 1000 kJ mol^{-1} nm^{-2}, gradually relaxed in five consecutive steps of 100 ps each, to 500,

200, 100 and 50 kJ mol^{-1} nm^{-2}. Four MD simulations with different initial poses of TMPyP4 (see Figure 4SI) were initially conducted for 100 ns for the binding of TMPyP4 with each DNA hybrid. The starting structures were obtained by the Maestro software [Maestro, version 10.2, Schrödinger, LLC, New York, NY, 2015]. Two final MD simulations were conducted for 300 ns and 200 ns, for the TMPyP4/F1K and TMPyP4/F2K systems, respectively.

3. Results and discussion.

UV-vis and ITC measurements were carried out to set the most adequate concentration range to conduct the kinetic study. Same experiments were performed in Na^+ and K^+ media to gather information about the similarities and differences of the studied system in the presence of these representative ions.

3.1. Isothermal Titration Calorimetry. ITC titrations of Tel22 (P) with increasing amounts of TMPyP4 (D) in 0.15 M NaCl and 0.15 M KCl were carried out. The profile of the titration isotherms (Fig. 1) shows two well differentiated steps. A general mechanism for this behavior is represented in eqns (1) and (2). For low C_D/C_P concentration ratios, the complex PD_1 gets formed (eqn (1)). As to the second process, PD_2 gets formed from PD_1 when the C_D/C_P ratio increases (eqn (2)), and is probably related to formation of external aggregates when the TMPyP4 concentration is raised.

$$P + D \underset{}{\overset{K_1}{\rightleftharpoons}} PD_1 \quad (1)$$

$$PD_1 + D \underset{}{\overset{K_2}{\rightleftharpoons}} PD_2 \quad (2)$$

The "two-site model" best fitted the experimental data, and the thermodynamic parameters obtained are listed in Table 1. The thermodynamic constant, K_1, for formation of PD_1 in the presence of K^+ was one order higher compared to Na^+, whereas with K_2 the opposite effect occurs. The reaction enthalpies were always negative. ΔH_1 varied with the type of buffer used, ΔH_1 (Na^+) < ΔH_1 (K^+), whereas ΔS_1 (Na^+) < 0 and ΔS_1 (K^+) > 0, indicating different hydration extent of the Tel22 conformations in Na^+ and K^+ buffers [38]. The ΔH_2 values remained nearly constant, whereas for the reaction entropy ΔS_2 (Na^+) > ΔS_2 (K^+) > 0, an effect attributed to dehydration of PD_1 to yield PD_2, in good agreement with formation of an external complex. The K_1 and K_2 values concur with those reported before in KCl buffer for the interaction of TMPyP4 and different types of human telomeric G-quadruplexes [24,39].

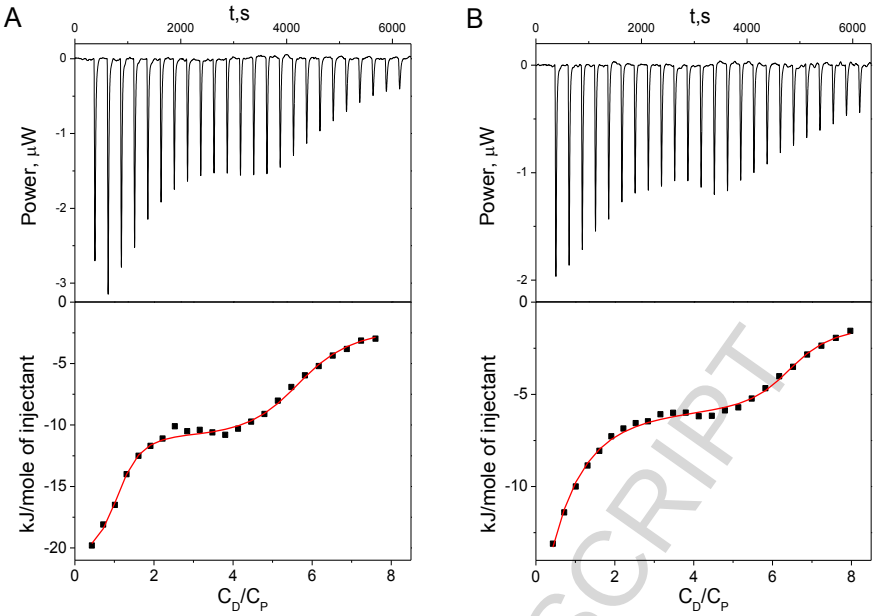

Fig. 1. ITC titrations of Tel22 with TMPyP4 in 0.15 M NaCl (**A**) and 0.15 M KCl (**B**). C^0_P = 0.065 mM, C^0_D = 1.7 mM, pH = 7.5 (10 mM Tris-HCl, 1 mM EDTA), T = 25 ºC**.**

Table 1. Thermodynamic parameters determined for the binding of TMPyP4 to Tel22 using a "two-site model". K_1 and K_2 are the thermodynamic constants and ΔH_1 and ΔH_2 the enthalpy change for the processes in eqns (1) and (2).

	10^{-5} K_1, M^{-1}	ΔH_1, kJ mol^{-1}	10^{-5} K_2, M^{-1}	ΔH_2, kJ mol^{-1}
Tel22/ TMPyP4[a]	1.6 ± 0.6	-45 ± 2	70 ± 30	-21 ± 2
Tel22/ TMPyP4[b]	25 ± 7	-15 ± 1	3.5 ± 0.9	-27 ± 1

a) 0.15 M NaCl and b) 0.15 M KCl

3.2. Spectrophotometric titration. The two differentiated processes observed with ITC measurements were also observed by spectrophotometric titrations of the Tel22/TMPyP4 system in 0.15 M NaCl (Fig. 2A) and 0.15 M KCl (Fig. 1SIA). The spectral curves recorded upon addition of increasing amounts of Tel22 to a TMPyP4 solution displayed a biphasic isotherm at λ = 433 nm with minimum at C_P/C_D = 0.5 (Fig. 2A, inset). An isosbestic point at λ = 429 nm with pronounced bathochromic shift of the maximum is observed for low TMPyP4 concentration (C_D/C_P < 2) (Fig. 2B), whereas for C_D/C_P > 2 a new isosbestic point at λ = 437 nm appears and the location of the maximum remains unaltered (Fig. 2C). This behaviour points to the existence of different types of Tel22/TMPyP4 complexes depending on the C_D/C_P concentration ratio, concurrent with the ITC results and with the scheme shown in eqns (1) and (2).

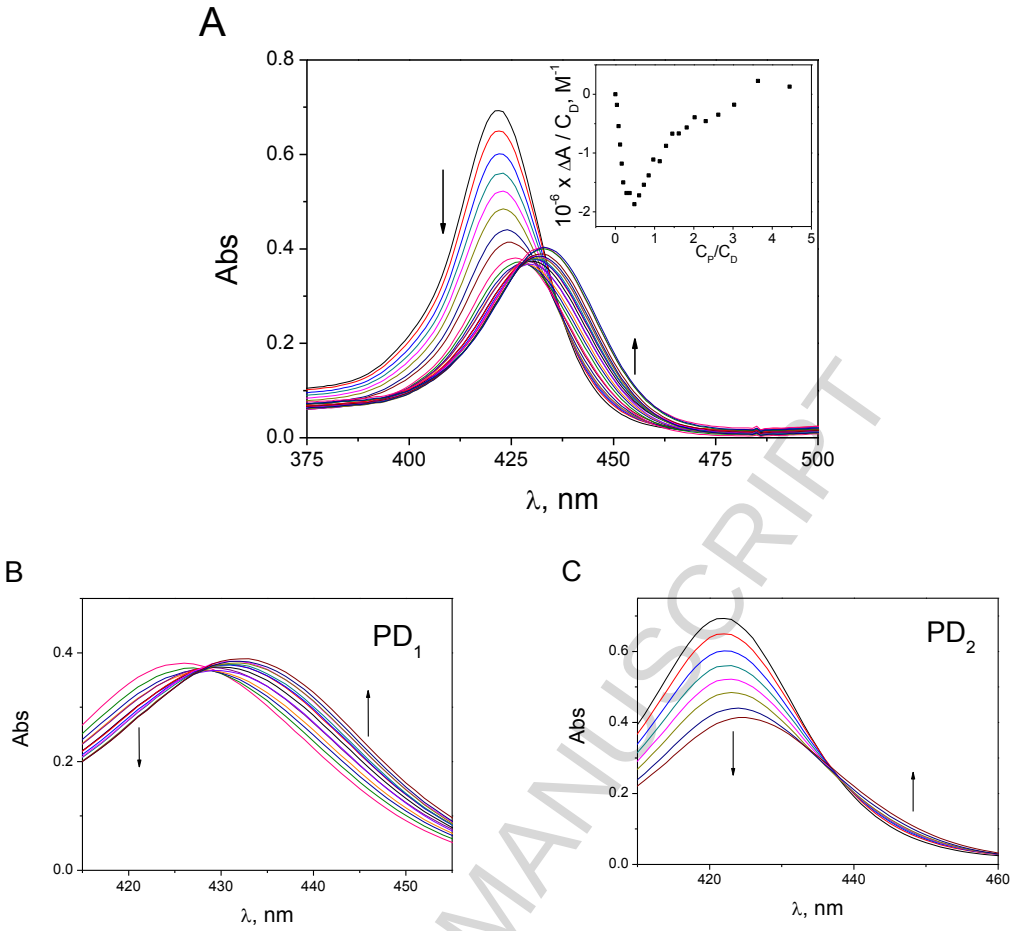

Fig. 2. Absorption spectra obtained from the titration of the TMPyP4/Tel22 system in 0.15 M NaCl. Inset: Binding isotherm at 433 nm (**A**). The spectral curves of Fig. 2A show two differentiated behaviours with two different isosbestic points at $C_D/C_P < 2$ (**B**) and at $C_D/C_P > 2$ (**C**). C^0_D = 3.5 μM, pH = 7.5 (10 mM Tris-HCl, 1 mM EDTA), T = 25 °C.

3.3. FRET melting measurements. A number of secondary structures, such as different G-quadruplex conformations, i-motifs and triplexes, can be present in solution for Tel22 and other important G-quadruplex sequences [11,40]. TMPyP4 promotes a notable increase in the melting temperature of G-quadruplex DNA structures [41]. Förster resonance energy transfer (FRET) melting experiments were carried out to obtain information about the main features of the Tel22/TMPyP4 interaction. Tel22 become perfectly stabilized upon binding with TMPyP4 both in Na^+ and K^+ buffers. Figs. 3A and 3B show the normalized FRET melting curves, whereas Fig. 3C and 3D show the T_m values determined in the mid-transition ($T_{1/2}$) for each C_D/C_P ratio. In the presence of TMPyP4, the ΔT_m value obtained for the dual fluorescently labeled (FAM and TAMRA) Tel22 oligonucleotide in the presence of Na^+ is equal to or greater than in the presence of K^+ for the same $\Delta(C_D/C_P)$, which reveals the influence of the ligand on the stabilization of different G-quadruplex Tel22 structures.

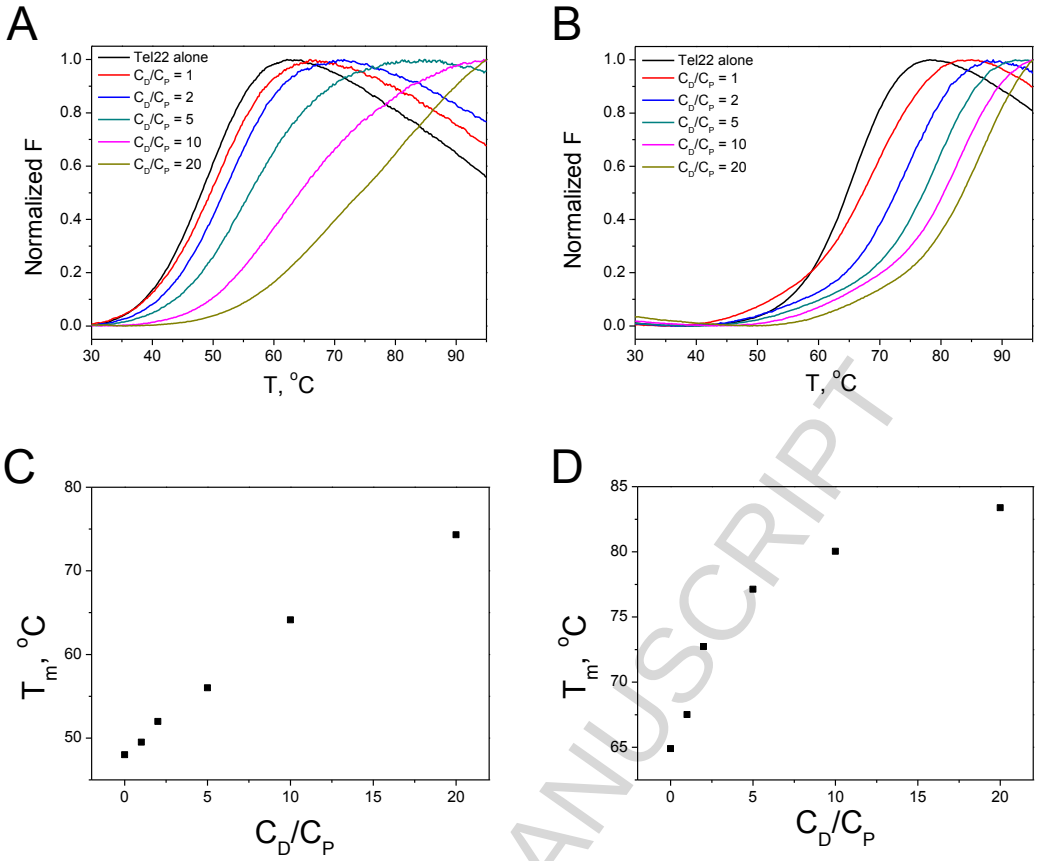

Fig. 3. FRET melting curves obtained for the TMPyP4/Tel22 system in 10 mM NaCl (**A**) and in 10 mM KCl (**B**) at different C_D/C_P ratios. Representation of the melting temperature (T_m) *versus* the C_D/C_P ratio in NaCl (**C**) and in KCl (**D**). C_P = 0.2 μM, pH = 7.5 (10 mM LiCaC, 90 mM LiCl).

3.4. Time-resolved fluorescence lifetime measurements. Fluorescence lifetime measurements have been widely used to study the existence and main features of ligand/G-quadruplex complexes [42]. The emission properties of the Tel22/TMPyP4 system were determined at different C_D/C_P ratios (Fig. 2SI). A monoexponential decay fitting was applied for free TMPyP4, whereas a biexponential fitting was needed to obtain acceptable χ^2 values when Tel22 is present. The τ_1 values were quite close to those of TMPyP4 alone, whereas the τ_2 values correspond to PD_1 (Table SI1). By means of this technique it was unfeasible to differentiate between different hybrid/TMPyP4 complexes, probably due to the close fluorescence lifetime values ascribable to their similar structure.

3.5. Kinetic T-Jump measurements. Thermodynamic data is valuable material to assess the final state of interacting systems, even though they cannot provide detailed mechanistic information. We studied the kinetic features of the Tel22/TMPyP4 interaction with the T-jump technique in the microsecond time scale to verify if the presence of the two different G-quadruplex conformations, F1M and F2M, entail any

significance on the way the ligands do interact with Tel22 in the presence of Na^+ and K^+. To this aim, T-jump measurements were performed for C_D/C_P ratio < 2, where PD_1 (eqn (1)) prevails. Kinetic measurements monitoring the absorbance were carried out at two different wavelengths, one at each side of the 429 nm isosbestic point. Fig. 4 collects examples of kinetic curves for the Tel22/TMPyP4 system in Na^+ and in K^+, recorded at 422 nm and 437 nm (see Figs. 2B and 1SIB). Single exponential functions were fitted to the experimental data (red line), from which the reciprocal relaxation time $1/\tau$ was obtained. Interestingly, the kinetics observed with equal concentration of Tel22 and TMPyP4 and same type of ion, showed that two reactions with quite different kinetic behaviour are at work. The faster reaction, which lasts less than 1 ms, could be observed at $\lambda = 437$ nm for both Na^+ and K^+ buffers (Figs. 4A and 4C, respectively), whereas the slower reaction can be followed at $\lambda = 422$ nm (Figs. 4B and 4D).

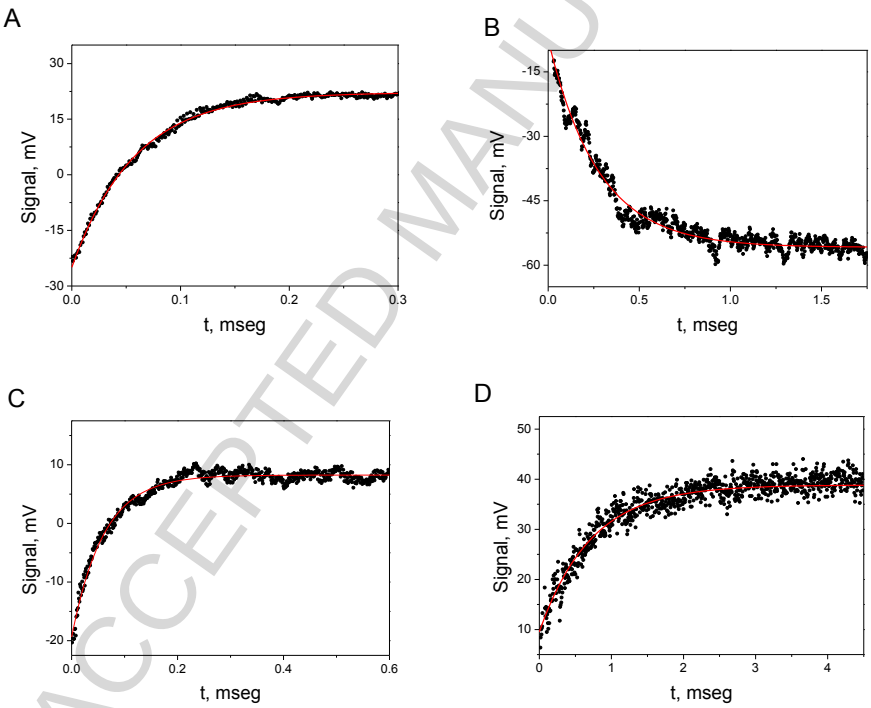

Fig. 4. Examples of kinetic curves obtained for the Tel22/TMPyP4 system in 0.15 M NaCl at $\lambda = 437$ nm (**A**) and $\lambda = 422$ nm (**B**) and in 0.15 M KCl at $\lambda = 437$ nm (**C**) and $\lambda = 422$ nm (**D**). $C_D = 3.5$ - 15 μM, $C_P = 6$ - 20 μM. pH = 7.5 (10 mM Tris-HCl, 1 mM EDTA), T = 25 ºC.

To obtain the forward and reverse kinetic constants of the four processes, plots of the reciprocal relaxation time ($1/\tau$) *versus* the equilibrium concentration function ([P] + [D]) (Fig. 5) were fitted according to eqn (3):

$$\frac{1}{\tau} = k_f \cdot ([P] + [D]) + k_d \qquad (3)$$

where k_f and k_d represent the formation and dissociation rate constants between Tel22 and TMPyP4 obtained at a specific wavelength.

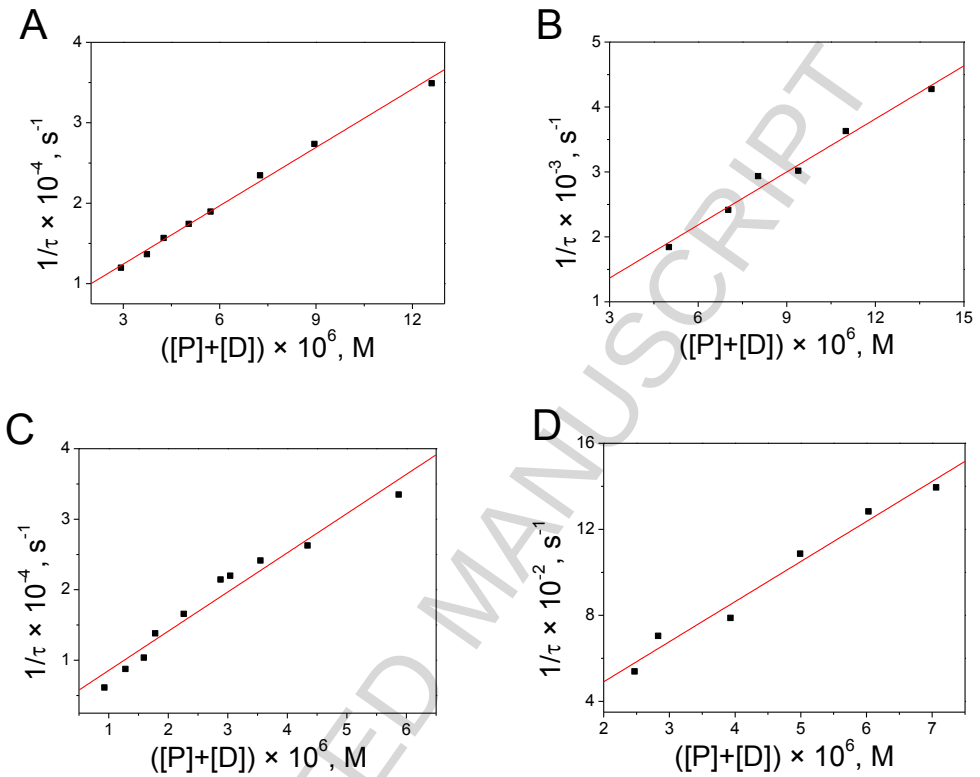

Fig. 5. (1/τ) *versus* ([P] + [D]) plot and fitting of eqn (3) to the data obtained for the Tel22/TMPyP4 system in 0.15 M NaCl at (**A**) λ = 437 nm, and (**B**) λ = 422 nm and in 0.15 M KCl at (**C**) λ = 437 nm and (**D**) λ = 422 nm.

Table 2 lists the rate constants together with the kinetic equilibrium constant, K_1, obtained from the ratio of the forward over the reverse kinetic constant ($k_{f,i}$ /$k_{d,i}$). The kinetic constants $k_{f,2}$ and $k_{d,2}$ obtained at 437 nm were one order higher than $k_{f,1}$ and $k_{d,1}$ obtained at 422 nm both in NaCl and KCl, whereas the thermodynamic value K_1 obtained at the two wavelengths are quite close for a particular buffer, being $K_1 \sim 4\times10^5\ M^{-1}$ and $2\times10^6\ M^{-1}$ in the presence of Na^+ and K^+ ions, respectively. This means that, although the two processes observed in the presence of each of the ions display well-differentiated kinetic behaviour, the overall thermodynamic equilibrium constant remains virtually unaffected. The binding constants concur fairly well with the

K_1 value obtained from the ITC measurements in Table 1 for formation of PD_1 (eqn (1)).

Table 2. Kinetic ($k_{f,i}$ and $k_{d,i}$) and thermodynamic ($K_1 = k_{f,i}/k_{d,i}$) constants of the equilibrium represented in eqns (4) and (5) for the Tel22/TMPyP4 system at low TMPyP4 concentration ($C_D/C_P < 2$).

	10^{-8} $k_{f,i}$, $M^{-1}s^{-1}$	10^{-2} $k_{d,i}$, s^{-1}	10^{-5} K_1, M^{-1}
F1Na/TMPyP4 (0.15 M NaCl)[1]	2.5 ± 0.2	5.5 ± 0.2	4.5 ± 0.2
F2Na/TMPyP4 (0.15 M NaCl)[2]	24.2 ± 0.6	52 ± 4	4.7 ± 2
F1K/TMPyP4 (0.15 M KCl)[1]	1.9 ± 0.1	1.2 ± 0.7	16± 1
F2K/TMPyP4 (0.15 M KCl)[2]	56 ± 4	30 ± 10	19 ± 7

1) λ = 422 nm; 2) λ = 437 nm

In conclusion, P in eqn (1) is the sum (F1M + F2M) and PD_1 is the sum (F1M/TMPyP4 + F2M/TMPyP4) in the presence of each M = Na^+ or K^+ ions. Therefore, the equilibrium in eqn (1) can be split into eqn (4) and eqn (5), $k_{f,i}$ and $k_{d,i}$ being the kinetic constants (Table 1) corresponding to two different conformations. However, so far the experimental results are insufficient to unambiguously assign the Tel22 conformation and the kinetic constants. This difficulty will be overcome below by means of the MD simulations.

$$\text{F1M} + \text{TMPyP4} \underset{k_{d,1}}{\overset{k_{f,1}}{\rightleftharpoons}} \text{F1M/TMPyP4} \qquad (4)$$

$$\text{F2M} + \text{TMPyP4} \underset{k_{d,2}}{\overset{k_{f,2}}{\rightleftharpoons}} \text{F2M/TMPyP4} \qquad (5)$$

Several other possible mechanisms could describe the kinetic data in terms of induced-fit and/or conformational selection pathways. However, on one side the existence of two hybrid forms in K^+ buffer (F1K and F2K) has been described amply (See, for instance, refs 10 and 11 and references therein), providing useful hints about the types of processes observed. On the other hand, if, together with the formation of the TMPyP4/Tel22 complexes, there would exist other T-jump processes, then some other complex reactions should be observed, prone to fitting with multiexponential functions. However, as a matter of fact single exponential functions sufficed to fit absolutely all the T-jump kinetic curves, which indicate that, under the different conditions studied, only a single kinetic process in the T-jump time scale is at work.

Likewise, the good linearity fulfilled by the different instances shown in Figure 5 reveals independent reactions from one another in every case.

To analyze the formation of PD_2 (eqn (2)), a number of T-Jump experiments were conducted in the concentrated region, $C_D/C_P \geq 2$, at different wavelengths around 422 nm, but no signals could be recorded, probably because the reaction is too fast to be observed by T-jump, which is compatible with the binding of additional TMPyP4 molecules to PD_1 to build the external complex PD_2.

As to the type of interaction of TMPyP4 with G quadruplex, different modes of binding have been proposed, including intercalation of the ligand between adjacent G-quartets, end-stacking on the external G-tetrads and groove-binding with external loops [20,22,43]. On one hand, the rather high k_d values obtained by T-jump measurements (Table 2) appear to be incompatible with intercalation of TMPyP4 into the G-tetrads, as the residence time is too short compared to other processes involving this mode of binding [44]. On the other hand, the pronounced red shift observed (Figs. 2B and 1SIB) indicates that PD_1 involves stacking between TMPyP4 and Tel22. This shift has been attributed to end-stacking of TMPyP4 on the external G-tetrads of the G-quadruplex [22,39]. However, the X-ray structure reported by Neidle et al. for human telomeric G-quadruplex/TMPyP4 complex has shown that TMPyP4 failed to directly interact with the external G-tetrad due to steric clashes between the G-tetrad edges and the N-methylpyridyl groups of TMPyP4 [21]. Instead, TMPyP4 established π-π interactions with external bases and electrostatic interactions between the cationic N-methylpyridyl groups and the phosphate ions of the telomeric DNA. Hence, MD simulations were carried out to shed light both on i) the distinct experimental kinetic behaviour observed as a consequence of the interaction of TMPyP4 with the two G-quadruplex conformations of Tel22, and ii) on the nature of its mode of binding.

3.6. MD simulations. The T-jump technique demonstrated quantitatively that the rates of formation of F1M/TMPyP4 and F2M/TMPyP4 were different, but it is unable to differentiate which of the two complexes gets formed faster. Moreover, the structural difference between F1M and F2M provides a convincing explanation for the different reaction rates which, notwithstanding, does not alter the affinity for TMPyP4, thus presenting very similar values of the affinity constants K_1. To discern this issue, explain the reasons for such a difference and shed some light into the binding features of the Tel22/TMPyP4 system, MD simulations were carried out using the well-characterized

hybrid Tel22 conformations in K^+. These two conformations display quite similar structure containing the same type and number of loops (one reversal and two lateral loops), but their arrangement is actually different. In the hybrid-1 (F1K), the 5' loop is in the reversed configuration, whereas in the hybrid-2 (F2K) the 3' loop is the one in the reversed configuration, as represented in Scheme 1 [40]. Fig. 3SI shows the optimized structure of TMPyP4, where the central aromatic moiety remains planar, while the methyl-pyridine groups can rotate nearly perpendicular to the molecular plane. The Root-Mean-Square Deviation (RMSD) plot, red line in Fig. 6, and the atom-atom distance between TMPyP4 and a selected nucleotide, blue line in Fig. 6, both enable one to follow the host-guest binding process occurring along the MD trajectory, where important conformational changes occur before and at the equilibrium phase. Different intermediate structures of the F1K/TMPyP4 and F2K/TMPyP4 complexes, occurring along the MD simulation are also shown (Figs. 6A and 6B), and describe the molecular recognition process until the equilibrium (plateau) is reached. In particular, the distance between one of the four pyrrole nitrogen atoms of TMPyP4 and one atom of the external bases, thymine O1 for F1K and adenine N1 for F2K, reveals that the final stacking distance between TMPyP4 and both DNA hybrids oscillates around 4 Å when the equilibrium phase has been reached. The initial and final position of TMPyP4 (gray) is shown in Fig. 7 (see also Fig 4SI for all considered starting positions). It can be observed that TMPyP4 binds to the nucleic acid through π-π stacking interactions with a nitrogen base in the groove (thymine in F1K and adenine in F2K). In addition, the methylpyridyl groups, positively charged, remain oriented towards the negatively charged phosphate groups of the G-quadruplex chain.

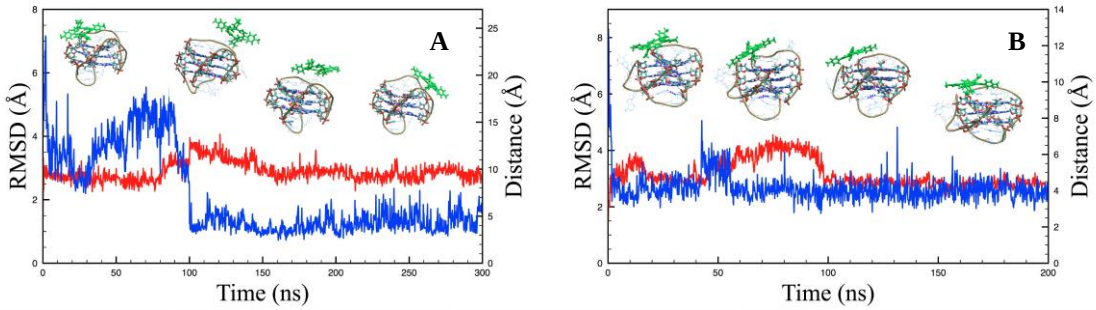

Fig. 6. RMSD plot (red) and specific distance between one of the four pyrrole nitrogen atoms of TMPyP4 and one atom of the binding base (blue) for the F1K/TMPyP4 (**A)** and the F2K/TMPyP4 system (**B**).

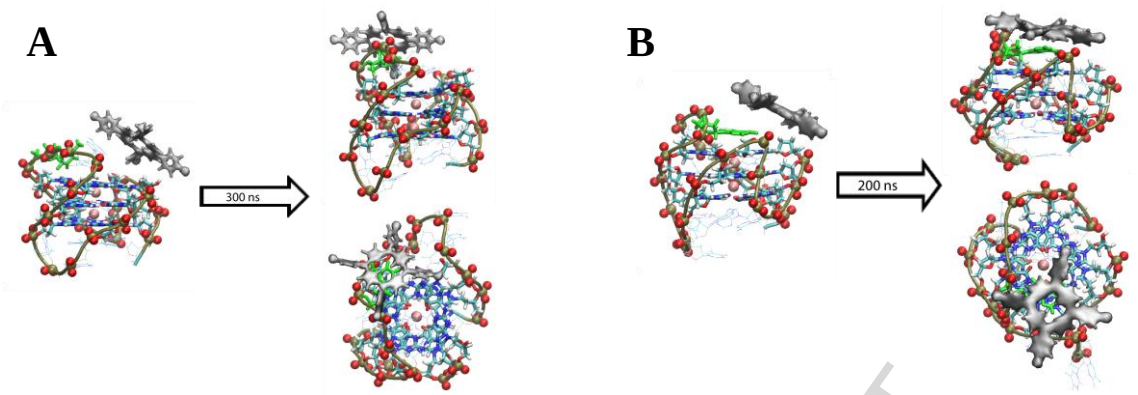

Fig. 7. Initial and final (top and side views) relative positions in the MD simulation of TMPyP4 (gray) and Tel22. Oxygen atoms in phosphate groups are represented as red balls; water and counterions have been removed. (**A**) Hybrid-1 F1K; the thymine base interacting with TMPyP4 is highlighted in green. (**B**) Hybrid-2 F2K; the adenine base interacting with TMPyP4 is highlighted in green.

The analysis of the experimental data demonstrates that the thermodynamics of the binding of TMPyP4 to F1K and F2K are similar, as indicated by the very close values of the thermodynamic constant, $K_1 = k_f / k_d$, of the equilibria represented in eqns (4) and (5). The results of the MD simulations provide a plausible explanation for such phenomena, as the binding mode and the final structure of the F1K/TMPyP4 complex and those of the F2K/TMPyP4 complex are closely akin (Fig. 7), which render them thermodynamically indistinguishable.

On the other hand, the values of the kinetic constants k_f and k_d indicate that one of the two binding processes is faster by one order of magnitude than the other (Table 2). Interestingly, remarkable differences were found in the molecular recognition process along the MD trajectory. In fact, Fig. 8 reveals that TMPyP4 binds rapidly to an adenine residue (highlighted green) in both hybrids, F1K and F2K, at roughly 2.5 ns. However, in the F2K/TMPyP4 system the binding to the adenine base persists up to the end of the simulation (Fig. 8A), so the equilibrium is attained faster. By contrast, an important change in the position of the ligand is observed at 101 ns for the F1K/TMPyP4 system (Fig. 8B). In particular, it is released from the binding site at the adenine base and binds to a thymine residue (highlighted yellow), finally reaching an equilibrium state. In our opinion, this difference can be related to the slower kinetics of binding experimentally observed by T-jump for one of the two hybrids.

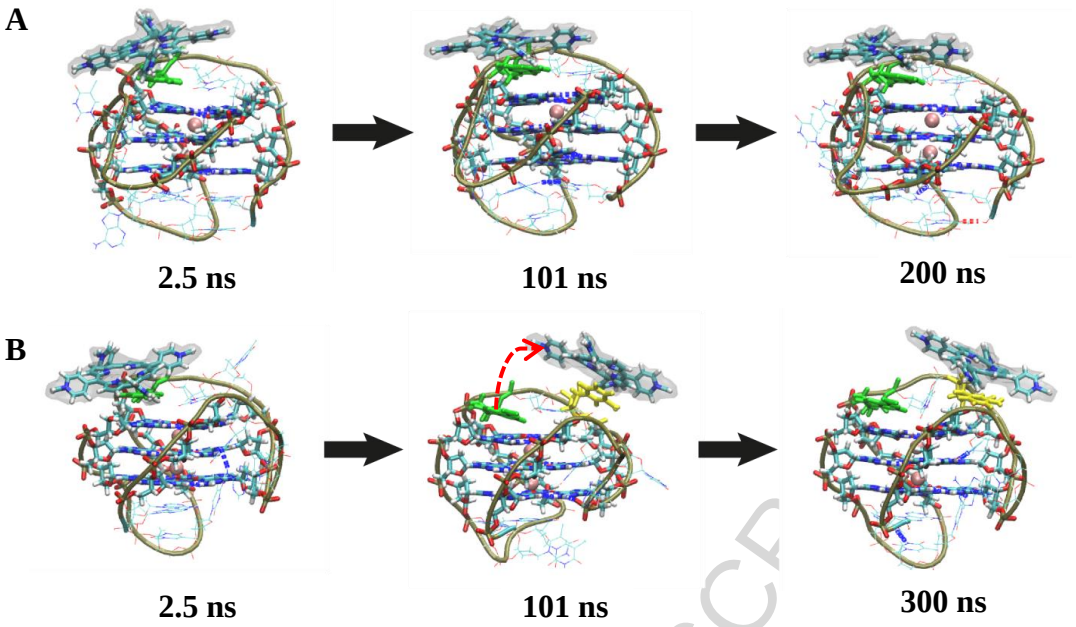

Fig. 8. Molecular recognition scheme during the MD simulation of the F2K/TMPyP4 system (**A**) and the F1K/TMPyP4 system (**B**).

In summary, the pathway observed during the molecular recognition process points to a difference in the time needed to reach the equilibrium structure for the F1K/TMPyP4 and F2K/TMPyP4 complexes. As k_f and k_d are directly related to the reciprocal time of formation and dissociation of the F1K/TMPyP4 and F2K/TMPyP4 complexes, the MD simulation results are in fairly good agreement with the two different experimental values observed for $k_{f,i}$ and $k_{d,i}$.

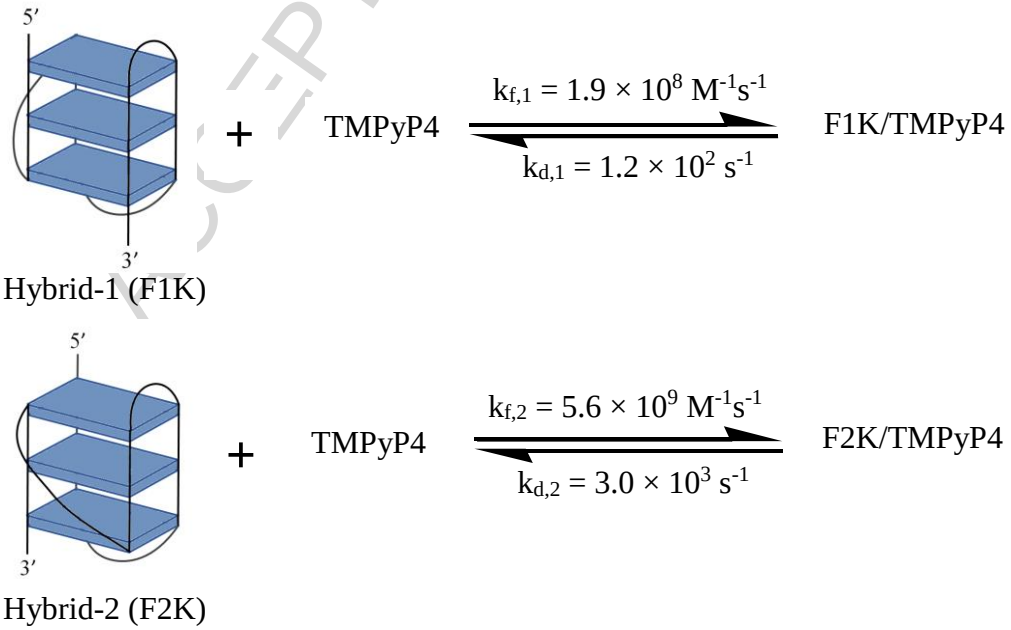

Scheme 1. Schematic representation of the kinetic behaviour of the Tel22/TMPyP4 system in K^+.

It also allows one to assess that, in the case of Tel22 in K^+, the faster kinetics involves the binding of TMPyP4 to the hybrid-2 form, F2K, whereas the slower kinetics is related to the binding of TMPyP4 to the hybrid-1 form, F1K. The $k_{f,i}$ and $k_{d,i}$ values of reactions 4 and 5 are defined and assigned in Scheme 1 for K^+ buffer.

The possibility of building different conformations from the same sequence is a complex issue that confers G-quadruplexes very interesting physical chemistry features. When the biological relevance of these conformations becomes well-known, we shall be aware of the importance conveyed by the fact that a ligand may stay more or less time bound to a particular G4 conformation. For example, in ligand/DNA intercalation reactions, slow dissociation rates are viewed as an important criterion regarding their efficiency as cancer therapeutics, because such drugs remain longer in the intercalation position and are assumed to alter the DNA transcription [45].

4. Conclusions.

We have shown for the first time by experimental measurements and molecular modeling that a small ligand such as the cationic porphyrin TMPyP4 interacts in a distinct way with the two forms of G-quadruplex present in solution for the human telomeric sequence Tel22, both in Na^+ and K^+ buffers. In fact, for a particular buffer, under the same experimental conditions, two different sets of rate constants (k_f and k_d) differing by one order of magnitude but yielding the same affinity constant $K_1 = k_f/k_d$ were observed. MD simulations performed with the Tel22 structures in the presence of K^+ ions suggest that the hybrid-2 reaches the equilibrium with TMPyP4 faster than with hybrid-1. However, the structural difference between the two final equilibrium complexes is small, rendering the two types of Tel22/TMPyP4 complex thermodynamically indistinguishable and accounting for the only thermodynamic constant value obtained for K_1. Moreover, it provides convincing explanation for the observation that, although the coexistence of different conformations in solution has been probed for several G-quadruplex sequences, only kinetic techniques can fully characterize the binding mechanism of small ligands to the different structures when the final equilibrium states are nearly equivalent.

Acknowledgements

The research leading to these results has received funding from "la Caixa" Foundation (project OSLC-2012-007), MINECO, Junta de Castilla y León, (CTQ2014-58812-C2-2-R and BU042U16, FEDER Funds, respectively) Spain, are gratefully acknowledged). C.P-A. is grateful for the FPU grant from Ministry of Education, Culture and Sports, Madrid, Spain (FPU13/00180).

References

[1] D. Monchaud, M.-P. Teulade-Fichou, A hitchhiker's guide to G-quadruplex ligands, Org. Biomol. Chem., 6 (2008) 627–636.

[2] P. Murat, S. Balasubramanian, Existence and consequences of G-quadruplex structures in DNA, Curr. Opin. Genet. Dev., 25 (2014) 22–29.

[3] V.S. Chambers, G. Marsico, J.M. Boutell, M. Di Antonio, G.P. Smith, S. Balasubramanian, High-throughput sequencing of DNA G-quadruplex structures in the human genome, Nat. Biotechnol., 33 (2015) 877–881.

[4] A. Bedrat, J.-L. Mergny, L. Lacroix, Re-evaluation of G-quadruplex propensity with G4Hunter, Nucleic Acids Res., 44 (2016) 1746–1759.

[5] S. Neidle, Human telomeric G-quadruplex: the current status of telomeric G-quadruplexes as therapeutic targets in human cancer, FEBS J., 277 (2010) 1118–1125.

[6] H. Lodish, A. Berk, C.A. Kaiser, M. Krieger, M.P. Scott, A. Bretscher, H. Ploegh, P. Matsudaira, Intracellular Ion Environment and Membrane Electric Potential, in: N.Y. W. H. Freeman (Ed.), Mol. Cell Biol., 4th ed., 2000.

[7] A. Ambrus, D. Chen, J. Dai, T. Bialis, R.A. Jones, D. Yang, Human telomeric sequence forms a hybrid-type intramolecular G-quadruplex structure with mixed parallel/antiparallel strands in potassium solution, Nucleic Acids Res., 34 (2006) 2723–2735.

[8] A.T. Phan, K.N. Luu, D.J. Patel, Different loop arrangements of intramolecular human telomeric (3+1) G-quadruplexes in K+ solution, Nucleic Acids Res., 34 (2006) 5715–5719.

[9] Y. Wang, D.J. Patel, Solution structure of the human telomeric repeat d[AG3(T2AG3)3]G-tetraplex, Struct., 1 (1993) 263–282.

[10] K.W. Lim, V.C.M. Ng, N. Martin-Pintado, B. Heddi, A.T. Phan, Structure of the human telomere in Na+ solution: an antiparallel (2+2) G-quadruplex scaffold

reveals additional diversity, Nucleic Acids Res., 41 (2013) 10556–10562.

[11] C. Perez-Arnaiz, N. Busto, J.M. Leal, B. Garcia, New microsecond intramolecular reactions of human telomeric DNA in solution, RSC Adv., 6 (2016) 39204–39208.

[12] M. Aznauryan, S. Sondergaard, S.L. Noer, B. Schiott, V. Birkedal, A direct view of the complex multi-pathway folding of telomeric G-quadruplexes, Nucleic Acids Res., 44 (2016) 11024–11032.

[13] J. Palacky, M. Vorlickova, I. Kejnovska, P. Mojzes, Polymorphism of human telomeric quadruplex structure controlled by DNA concentration: a Raman study, Nucleic Acids Res., 41 (2013) 1005–1016.

[14] J. Sponer, G. Bussi, P. Stadlbauer, P. Kuhrova, P. Banas, B. Islam, S. Haider, S. Neidle, M. Otyepka, Folding of guanine quadruplex molecules-funnel-like mechanism or kinetic partitioning? An overview from MD simulation studies, Biochim. Biophys. Acta, Gen. Subj., 1861 (2017) 1246–1263.

[15] M. Boncina, G. Vesnaver, J.B. Chaires, J. Lah, Unraveling the Thermodynamics of the Folding and Interconversion of Human Telomere G-Quadruplexes, Angew. Chemie, Int. Ed., 55 (2016) 10340–10344.

[16] R.T. Wheelhouse, D. Sun, H. Han, F.X. Han, L.H. Hurley, Cationic Porphyrins as Telomerase Inhibitors: the Interaction of Tetra(N-methyl-4-pyridyl)porphine with Quadruplex DNA, J. Am. Chem. Soc., 120 (1998) 3261–3262.

[17] T.L. Ruan, S.J. Davis, B.M. Powell, C.P. Harbeck, J. Habdas, P. Habdas, L.A. Yatsunyk, Lowering the overall charge on TMPyP4 improves its selectivity for G-quadruplex DNA, Biochimie, 132 (2017) 121–130.

[18] A.J. Gaier, D.R. McMillin, Binding Studies of G-Quadruplex DNA and Porphyrins: Cu(T4) vs Sterically Friendly Cu(tD4), Inorg. Chem., 54 (2015) 4504–4511.

[19] J.I. DuPont, K.L. Henderson, A. Metz, V.H. Le, J.P. Emerson, E.A. Lewis, Calorimetric and spectroscopic investigations of the binding of metallated porphyrins to G-quadruplex DNA, Biochim. Biophys. Acta, Gen. Subj., 1860 (2016) 902–909.

[20] I. Haq, J.O. Trent, B.Z. Chowdhry, T.C. Jenkins, Intercalative G-Tetraplex Stabilization of Telomeric DNA by a Cationic Porphyrin, J. Am. Chem. Soc., 121 (1999) 1768–1779.

[21] G.N. Parkinson, R. Ghosh, S. Neidle, Structural Basis for Binding of Porphyrin

to Human Telomeres, Biochemistry, 46 (2007) 2390–2397.

[22] C. Wei, G. Jia, J. Zhou, G. Han, C. Li, Evidence for the binding mode of porphyrins to G-quadruplex DNA, Phys. Chem. Chem. Phys., 11 (2009) 4025–4032.

[23] M. Boncina, C. Podlipnik, I. Piantanida, J. Eilmes, M.-P. Teulade-Fichou, G. Vesnaver, J. Lah, Thermodynamic fingerprints of ligand binding to human telomeric G-quadruplexes, Nucleic Acids Res., 43 (2015) 10376–10386.

[24] L. Martino, B. Pagano, I. Fotticchia, S. Neidle, C. Giancola, Shedding Light on the Interaction between TMPyP4 and Human Telomeric Quadruplexes, J. Phys. Chem. B, 113 (2009) 14779–14786.

[25] R. Rigler, C.R. Rabl, T.M. Jovin, Temperature-jump apparatus for fluorescence measurements, Rev. Sci. Instrum., 45 (1974) 580–588.

[26] J. Dai, C. Punchihewa, A. Ambrus, D. Chen, R.A. Jones, D. Yang, Structure of the intramolecular human telomeric G-quadruplex in potassium solution: a novel adenine triple formation, Nucleic Acids Res., 35 (2007) 2440–2450.

[27] J.J.P. Stewart, Optimization of parameters for semiempirical methods V: modification of NDDO approximations and application to 70 elements, J. Mol. Model., 13 (2007) 1173–1213.

[28] Y. Zhao, D.G. Truhlar, The M06 suite of density functionals for main group thermochemistry, thermochemical kinetics, noncovalent interactions, excited states, and transition elements: two new functionals and systematic testing of four M06-class functionals and 12 other function, Theor. Chem. Acc., 120 (2008) 215–241.

[29] V. Barone, M. Cossi, Quantum Calculation of Molecular Energies and Energy Gradients in Solution by a Conductor Solvent Model, J. Phys. Chem. A, 102 (1998) 1995–2001.

[30] M. Cossi, N. Rega, G. Scalmani, V. Barone, Energies, structures, and electronic properties of molecules in solution with the C-PCM solvation model, J. Comput. Chem., 24 (2003) 669–681.

[31] J. Wang, R.M. Wolf, J.W. Caldwell, P.A. Kollman, D.A. Case, Development and testing of a general Amber force field, J. Comput. Chem., 25 (2004) 1157–1174.

[32] J. Wang, W. Wang, P.A. Kollman, D.A. Case, Automatic atom type and bond type perception in molecular mechanical calculations, J. Mol. Graph. Model., 25 (2006) 247–260.

[33] A.T. Guy, T.J. Piggot, S. Khalid, Single-stranded DNA within nanopores: Conformational dynamics and implications for sequencing; a molecular dynamics simulation study, Biophys. J., 103 (2012) 1028–1036.

[34] D. Van Der Spoel, E. Lindahl, B. Hess, G. Groenhof, A.E. Mark, H.J.C. Berendsen, GROMACS: Fast, flexible, and free, J. Comput. Chem., 26 (2005) 1701–1718.

[35] B. Hess, C. Kutzner, D. van der Spoel, E. Lindahl, GROMACS 4: Algorithms for Highly Efficient, Load-Balanced, and Scalable Molecular Simulation, J. Chem. Theory Comput., 4 (2008) 435–447.

[36] G. Bussi, D. Donadio, M. Parrinello, Canonical sampling through velocity rescaling, J. Chem. Phys., 126 (2007) 014101/1-014101/7.

[37] T. Darden, D. York, L. Pedersen, Particle mesh Ewald: an N·log(N) method for Ewald sums in large systems, J. Chem. Phys., 98 (1993) 10089–10092.

[38] I. Jelesarov, H.R. Bosshard, Isothermal titration calorimetry and differential scanning calorimetry as complementary tools to investigate the energetics of biomolecular recognition, J. Mol. Recognit., 12 (1999) 3–18.

[39] A. Arora, S. Maiti, Effect of Loop Orientation on Quadruplex-TMPyP4 Interaction, J. Phys. Chem. B, 112 (2008) 8151–8159.

[40] R.D. Gray, J.O. Trent, J.B. Chaires, Folding and Unfolding Pathways of the Human Telomeric G-Quadruplex, J. Mol. Biol., 426 (2014) 1629–1650.

[41] A. De Rache, J.-L. Mergny, Assessment of selectivity of G-quadruplex ligands via an optimised FRET melting assay, Biochimie, 115 (2015) 194–202.

[42] A. Spinello, G. Barone, J. Grunenberg, Molecular recognition of naphthalene diimide ligands by telomeric quadruplex-DNA: the importance of the protonation state and mediated hydrogen bonds, Phys. Chem. Chem. Phys., 18 (2016) 2871–2877.

[43] C. Wei, G. Jia, J. Yuan, Z. Feng, C. Li, A Spectroscopic Study on the Interactions of Porphyrin with G-Quadruplex DNAs, Biochemistry, 45 (2006) 6681–6691.

[44] W.D. Wilson, C.R. Krishnamoorthy, Y.H. Wang, J.C. Smith, Mechanism of intercalation: ion effects on the equilibrium and kinetic constants for the interaction of propidium and ethidium with DNA, Biopolymers, 24 (1985) 1941–1961.

[45] A. Rhoden Smith, B.L. Iverson, Threading Polyintercalators with Extremely Slow Dissociation Rates and Extended DNA Binding Sites, J. Am. Chem. Soc.,

135 (2013) 12783–12789.

Conflict of interest

The authors have no conflict of interest to declare.

Highlights

- Reaction of TMPyP4 with hybrid-1 and hybrid-2 Tel22 telomeric conformations are observed
- The formation and dissociation reaction rates require T-jump to be monitored
- The fastest reaction in K^+ buffer involves hybrid-1
- TMPyP4 binds to the G-quadruplex groove with hybrid-1 and hybrid-2
- TMPyP4/Tel22 complexes are thermodynamically indiscernible in a particular buffer